



Cite this: *CrystEngComm*, 2021, 23, 1578

## Insight into non-covalent interactions in two triamine-based mononuclear iron(III) Schiff base complexes with special emphasis on the formation of Br $\cdots\pi$ halogen bonding†

Tanmoy Basak,<sup>a</sup> Antonio Frontera <sup>\*b</sup> and Shouvik Chattopadhyay <sup>\*a</sup>

Two mononuclear iron(III) complexes, [FeL<sup>1</sup>Cl]·CH<sub>3</sub>CN (**1**) and [FeL<sup>2</sup>(N<sub>3</sub>)] (**2**) {H<sub>2</sub>L<sup>1</sup> = *N,N'*-bis(5-chlorosalicylidene)diethylenetriamine and H<sub>2</sub>L<sup>2</sup> = *N,N'*-bis(5-bromosalicylidene)diethylenetriamine}, have been synthesized and characterized by X-ray crystallographic studies. In the solid state, there are strong hydrogen bonding interactions in both complexes due to the presence of the Fe(III)-coordinated amino group and anionic ligands, which are strong hydrogen bond donors and acceptors, respectively. These interactions have been studied by means of DFT and QTAIM calculations. Moreover, in the complex **2**, the formation of halogen bonding interactions (Br $\cdots\pi$ ) has been analyzed. The MEP analysis evidences the existence of a  $\sigma$ -hole at the bromine atom, and the concomitant Br $\cdots\pi$  interaction has been confirmed by QTAIM analysis.

Received 20th October 2020,  
Accepted 5th January 2021

DOI: 10.1039/d0ce01534b

rsc.li/crystengcomm

### Introduction

The use of metal complexes of Schiff bases as molecular magnets, as catalysts, and as liquid crystals has been well established since long.<sup>1</sup> Salen-type Schiff bases are used in most cases to form mono and polynuclear complexes of different transition and non-transition metals.<sup>2</sup> Focussing on iron(III), many Fe(III)-salen complexes have shown various catalytic activities using vacant or labile axial sites, especially in solution.<sup>3</sup> Oxo-bridged iron(III) dimeric complexes of salen are also very important for their relevance to different metalloproteins and metallo-enzymes.<sup>4</sup> However, compared with the large number of Fe(III)-salen complexes,<sup>5</sup> the literature shows only limited Fe(III) complex examples of 'triamine-based' salen-type di-Schiff bases.<sup>6</sup> In this work, two triamine-based (salen type) Schiff base complexes of iron(III) have been synthesized and characterized. X-ray crystal structure determinations have established their structures. We concentrated on the solid state supramolecular interactions in these complexes.

Hydrogen bonding, C–H $\cdots\pi$ ,  $\pi\cdots\pi$ , cation $\cdots\pi$ , lone pair $\cdots\pi$  and anion $\cdots\pi$  interactions are very powerful tools in building supramolecular architectures.<sup>7a-f</sup> These weak intermolecular interactions have been shown to have very important roles in crystal engineering, biology, catalysis, *etc.*<sup>7g</sup> On the other hand,  $\sigma$ -hole (and  $\pi$ -hole) interactions are relatively new; however, they are currently becoming interesting players.<sup>7f</sup> The anisotropic distribution of the electron density may create a positive electrostatic region on an atom. Positive electrostatic areas formed along an  $\sigma$ -skeleton or in its perpendicular direction are called  $\sigma$ -holes or  $\pi$ -holes, respectively.<sup>7d-j</sup> The interactions of  $\sigma$ -holes or  $\pi$ -holes with electron-rich centers are recognized as  $\sigma$ -hole or  $\pi$ -hole interactions, respectively. The size and electron deficiency of  $\sigma$ -holes increase with increase in the polarizability of electron acceptor atoms. When a heavy atom (of groups IV to VII) is covalently bonded to an electronegative atom, the possibility of identifying strong  $\sigma$ -hole interactions increases.<sup>8</sup>

In the present work, we have used two halosalicylaldehydes to form two salen-type Schiff bases, which in turn are used to form two iron(III) complexes, [FeL<sup>1</sup>-Cl]·CH<sub>3</sub>CN (**1**) and [FeL<sup>2</sup>(N<sub>3</sub>)] (**2**) [H<sub>2</sub>L<sup>1</sup> = *N,N'*-bis(5-chlorosalicylidene)diethylenetriamine; H<sub>2</sub>L<sup>2</sup> = *N,N'*-bis(5-bromosalicylidene)diethylenetriamine]. In the solid state, there are strong H-bonding interactions in both complexes due to the presence of the Fe(III)-coordinated amino group and anionic ligands, which are strong H-bond donors and acceptors, respectively. These interactions have been studied by means of DFT and QTAIM calculations. The formation of

<sup>a</sup> Department of Chemistry, Inorganic Section, Jadavpur University, Kolkata 700032, India. E-mail: shouvik.chem@gmail.com

<sup>b</sup> Departamento de Química, Universitat de les Illes Balears, Crta. de Valldemossa km 7.5, 07122 Palma, Balears, Spain. E-mail: toni.frontera@uib.es

† Electronic supplementary information (ESI) available. CCDC 2036444 and 2036445 contain the supplementary crystallographic data for the complex. For ESI and crystallographic data in CIF or other electronic format see DOI: 10.1039/d0ce01534b

a Br $\cdots\pi$  halogen bond observed in the solid state of complex **2** has also been analyzed by QTAIM/NCI plot analysis. This is in good agreement with the MEP surface of complex **2**, which shows the existence of a  $\sigma$ -hole at the Br-atom and a negative potential over the aromatic ring. A supramolecular dimer is formed and the dimerization energy is modest, as expected for the moderately positive MEP value at the  $\sigma$ -hole.

## Experimental

### Materials

All chemicals were of reagent grade and used as purchased from Sigma-Aldrich without further purification.

**Caution!!!** Although no problems were encountered in this work, organic ligands in the presence of azides are potentially explosive. Only a small amount of the material should be prepared, and it should be handled with care.

### Preparation

**Preparation of ligands.** Two N<sub>3</sub>O<sub>2</sub>-donor pentadentate Schiff bases were prepared by reacting different aldehydes (5-chlorosalicylaldehyde and 5-bromosalicylaldehyde) with diethyltri-amine. Aldehydes and triamines were taken in a 2 : 1 ratio in acetonitrile and refluxed to prepare the following Schiff bases: *N,N'*-bis(5-chlorosalicylidene)diethylenetriamine (H<sub>2</sub>L<sup>1</sup>) and *N,N'*-bis(5-bromosalicylidene)diethylenetriamine (H<sub>2</sub>L<sup>2</sup>). The ligands were not isolated, and the acetonitrile solutions of these ligands were used directly for the syntheses of complexes **1** and **2**.

#### Preparation of the complexes

**[FeL<sup>1</sup>Cl]-CH<sub>3</sub>CN (1).** An acetonitrile solution of iron(III) chloride hydrate (~1 mmol, 0.170 g) was added to an acetonitrile solution of the Schiff base ligand (H<sub>2</sub>L<sup>1</sup>) separately under refluxing conditions. The mixture was maintained in open atmosphere at room temperature for 2 days. The dark crystalline product was collected by filtration. X-ray quality single crystals were collected from this crystalline product.

Yield: 0.357 g, ~70% (based on iron). Anal. calc. for C<sub>18</sub>H<sub>17</sub>-Cl<sub>3</sub>FeN<sub>3</sub>O<sub>2</sub>CH<sub>3</sub>CN (510.60): C, 47.05; H, 3.95; N, 10.97%. Found: C, 46.9; H, 3.8; N, 11.0%. FT-IR (KBr, cm<sup>-1</sup>): 3230 ( $\nu_{\text{N-H}}$ ); 1626 ( $\nu_{\text{C=N}}$ ).  $\lambda_{\text{max}}$  (nm) [ $\epsilon_{\text{max}}$  (lit mol<sup>-1</sup> cm<sup>-1</sup>)] (acetonitrile): 501 (1.53  $\times 10^3$ ), 318 (3.68  $\times 10^3$ ), 228 (1.63  $\times 10^4$ ).

**[FeL<sup>2</sup>(N<sub>3</sub>)] (2).** An acetonitrile solution of iron(III) chloride hydrate (~1 mmol, 0.170 g) was added to an acetonitrile solution of the Schiff base ligand (H<sub>2</sub>L<sup>2</sup>) under refluxing conditions. An aqueous solution of sodium azide (~1 mmol, 0.070 g) was then added to the mixture, which was refluxed further for ca. 30 min. The mixture was maintained in open atmosphere at room temperature for 2 days. The dark crystalline product was collected by filtration. X-ray quality single crystals were collected from this crystalline product.

Yield: 0.423 g, ~75% (based on iron). Anal. calc. for C<sub>18</sub>-H<sub>17</sub>Br<sub>2</sub>FeN<sub>6</sub>O<sub>2</sub> (565.03): C, 53.35; H, 5.49; N, 16.97%. Found: C, 53.2; H, 5.3; N, 17.1%. FT-IR (KBr, cm<sup>-1</sup>): 3223 ( $\nu_{\text{N-H}}$ ); 2927–2837 ( $\nu_{\text{C-H}}$ ); 2073 ( $\nu_{\text{N}_3}$ ); 1623 ( $\nu_{\text{C=N}}$ ).  $\lambda_{\text{max}}$  (nm) [ $\epsilon_{\text{max}}$  (lit

mol<sup>-1</sup> cm<sup>-1</sup>)] (acetonitrile): 486 (1.60  $\times 10^3$ ), 307 (2.99  $\times 10^3$ ), 225 (1.48  $\times 10^4$ ).

### Physical measurements

Elemental analysis (carbon, hydrogen and nitrogen) was performed using a Perkin-Elmer 240C elemental analyzer. IR spectra in KBr (4500–500 cm<sup>-1</sup>) were recorded with a Perkin-Elmer Spectrum Two spectrophotometer. Electronic spectra in acetonitrile were recorded on a Shimadzu UV-1700 spectrophotometer.

### X-ray crystallography

Suitable crystals of complexes **1** and **2** were used for data collection using a Bruker D8 QUEST area detector diffractometer equipped with graphite-monochromated Mo K $\alpha$  radiation ( $\lambda = 0.71073$  Å). Molecular structures were solved by direct methods and refined by full-matrix least squares on  $F^2$  using the SHELX-18 package.<sup>9</sup> Non-hydrogen atoms were refined with anisotropic thermal parameters. The hydrogen atoms attached to nitrogen atoms were located by difference Fourier maps and were maintained at fixed positions. All other hydrogen atoms were placed in their geometrically idealized positions and constrained to ride on their parent atoms. Multi-scan empirical absorption corrections were applied to the data using the program SADABS.<sup>10</sup> The details of the crystallographic data and refinements are given in Table 1. Selected bond lengths and bond angles are listed in Tables 2 and 3, respectively.

### Theoretical methods

The calculations of the non-covalent interactions were performed using Gaussian-16 (ref. 11) at the PBE0-D3/def2-TZVP level of theory. The dimerization energies reported herein have been corrected using the standard Boys and Bernardi

**Table 1** Crystal data and refinement details of complexes **1** and **2**

Complex	<b>1</b>	<b>2</b>
Formula	C <sub>18</sub> H <sub>17</sub> Cl <sub>3</sub> FeN <sub>3</sub> O <sub>2</sub> , CH <sub>3</sub> CN	C <sub>18</sub> H <sub>17</sub> Br <sub>2</sub> FeN <sub>6</sub> O <sub>2</sub>
Formula weight	510.60	565.03
Temperature (K)	273	273
Crystal system	Monoclinic	Monoclinic
Space group	<i>P</i> <sub>2</sub> <sub>1</sub> / <i>n</i>	<i>P</i> <sub>2</sub> <sub>1</sub> / <i>n</i>
<i>a</i> (Å)	13.642(2)	12.7967(10)
<i>b</i> (Å)	12.843(2)	9.4429(7)
<i>c</i> (Å)	13.658(2)	17.7657(14)
$\alpha$ (°)	90	90
$\beta$ (°)	107.055(5)	108.017(3)
$\gamma$ (°)	90	90
<i>Z</i>	4	4
<i>d</i> <sub>cal</sub> (g cm <sup>-3</sup> )	1.482	1.838
$\mu$ (mm <sup>-1</sup> )	1.033	4.681
<i>F</i> (000)	1044	1116
Total reflection	76 272	27 652
Unique reflections	5222	4215
Observe data [ <i>I</i> > 2 $\sigma$ ( <i>I</i> )]	4818	3407
<i>R</i> (int)	0.040	0.051
<i>R</i> <sub>1</sub> , <i>wR</i> <sub>2</sub> (all data)	0.0457, 0.1339	0.0498, 0.0897
<i>R</i> <sub>1</sub> , <i>wR</i> <sub>2</sub> [ <i>I</i> > 2 $\sigma$ ( <i>I</i> )]	0.0405, 0.1210	0.0359, 0.0826

**Table 2** Selected bond lengths (Å) of complexes **1** and **2**

Complex	1	2
Fe(1)–O(1)	1.9231(17)	1.959(2)
Fe(1)–O(2)	1.9349(18)	1.939(2)
Fe(1)–N(1)	2.1800(19)	2.121(3)
Fe(1)–N(2)	2.250(2)	2.245(3)
Fe(1)–N(3)	2.107(2)	2.178(3)
Fe(1)–N(4)	—	1.988(3)
Fe(1)–Cl(3)	2.3408(8)	—

**Table 3** Selected bond angles (°) of complexes **1** and **2**

Complex	1	2
O(1)–Fe(1)–O(2)	93.85(7)	90.97(10)
O(1)–Fe(1)–N(1)	84.84(7)	83.16(10)
O(1)–Fe(1)–N(2)	154.91(8)	108.03(12)
O(1)–Fe(1)–N(3)	93.79(8)	174.53(10)
O(1)–Fe(1)–N(4)	—	93.77(12)
O(2)–Fe(1)–N(1)	176.46(7)	94.97(11)
O(2)–Fe(1)–N(2)	107.35(8)	156.78(12)
O(2)–Fe(1)–N(3)	84.34(8)	84.61(10)
O(2)–Fe(1)–N(4)	—	103.23(13)
N(1)–Fe(1)–N(2)	74.73(8)	74.82(11)
N(1)–Fe(1)–N(3)	99.02(8)	93.99(11)
N(1)–Fe(1)–N(4)	75.59(8)	161.61(13)
N(2)–Fe(1)–N(3)	—	75.56(12)
N(2)–Fe(1)–N(4)	—	89.05(12)
N(3)–Fe(1)–N(4)	—	90.39(13)
Cl(3)–Fe(1)–O(1)	103.30(6)	—
Cl(3)–Fe(1)–O(2)	86.64(5)	—
Cl(3)–Fe(1)–N(1)	90.46(5)	—
Cl(3)–Fe(1)–N(2)	91.45(6)	—
Cl(3)–Fe(1)–N(3)	161.16(6)	—

counterpoise method.<sup>12</sup> The BSSE corrected interaction energy was evaluated by the following equations, where *A* and *B* indicate the monomer geometries and \* indicates the monomer geometries in the complex; a and b indicate the monomer basis set.  $E^{\text{CP}}$  is the additive correction energy. The  $E(A^*)_{\text{ab}}$  and  $E(B^*)_{\text{ab}}$  terms are evaluated through calculations with ghost orbitals as implemented in Gaussian-16 *via* the keyword counterpoise. It should be mentioned that the systems studied in this work are homodimers; therefore,  $A = B$ .

$$\Delta E_{\text{complex}} = E(A^*B^*)_{\text{ab}} - E(A)_a - E(B)_b \quad (1)$$

$$E^{\text{CP}} = E(A^*)_a - E(A^*)_{\text{ab}} + E(B^*)_b - E(B^*)_{\text{ab}} \quad (2)$$

Grimme's D3 dispersion correction was used in the calculations.<sup>13</sup> To evaluate the interactions in the solid state, the crystallographic coordinates were used, and only the position of the hydrogen bonds has been optimized. We have not used fully relaxed geometries because we are interested in evaluating the interactions as they stand in the solid state instead of finding the most global minimum energy of the complex. This procedure and level of theory has been used before to investigate non-covalent interactions in the solid state.<sup>14</sup> The QTAIM analysis<sup>15</sup> and NCI plot index<sup>16</sup> have been computed at the PBE0-D3/def2-TZVP level of theory by means

of the AIMAll program.<sup>17</sup> A comprehensive treatment of the QTAIM theory is provided in the literature.<sup>15</sup> The NCI plot index is an appropriate computational tool for the easy and efficient visualization and identification of NCIs. It is based on the fact that the non-covalent contacts can be identified with the peaks that emerge in the RDG (reduced density gradient) at low densities.<sup>16</sup> These are plotted in real space by mapping an isosurface of  $s$  ( $s = |\nabla\rho|/\rho^{4/3}$ ) for a low value of RDG. Upon formation of a supramolecular dimer, the RDG changes at the critical points in between the monomers due to the annihilation of the density gradient at these points. Therefore, the NCI plot index enables visualization of the extent to which NCIs stabilize a supramolecular assembly. The information that the NCI plot index provides is qualitative, revealing which molecular regions interact. The color scheme is a red-yellow-green-blue scale, with red for repulsive ( $\rho_{\text{cut}}^+$ ) and blue for attractive ( $\rho_{\text{cut}}^-$ ). Weak repulsive and weak attractive forces are represented by yellow and green surfaces, respectively.

The MEP calculations were carried out using the PBE0-D3/def2-TZVP level of theory and plotted using the Gaussview program.<sup>11</sup> The 0.001 a.u. isosurface has been used as a van der Waals envelope for building the MEP surfaces.

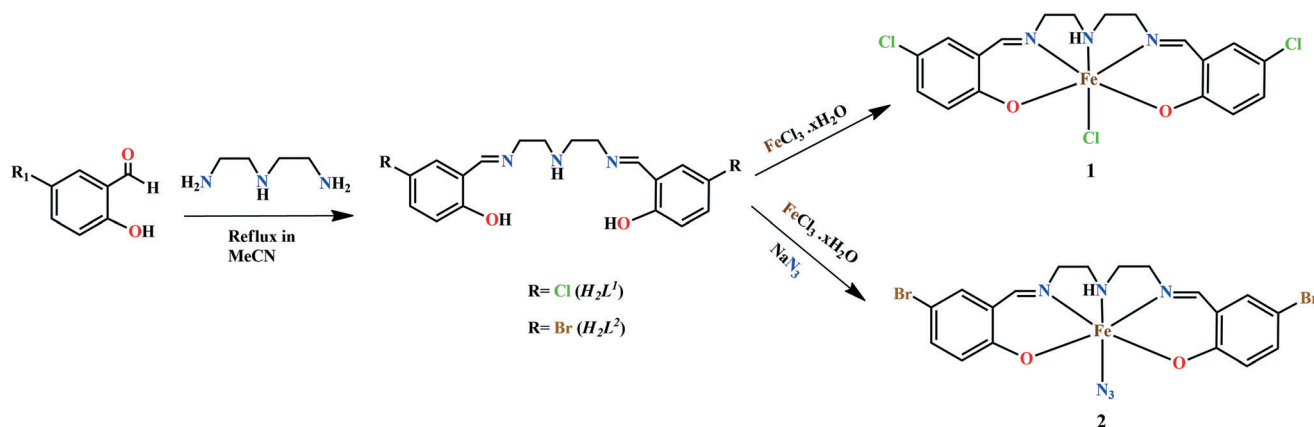
## Results and discussion

### Synthesis

The Schiff base ligands,  $\text{H}_2\text{L}^1$  and  $\text{H}_2\text{L}^2$ , were prepared by 1 : 2 condensation of diethyltriamine with 5-chlorosalicylaldehyde and 5-bromosalicylaldehyde, respectively, in acetonitrile.<sup>18</sup> The acetonitrile solution of each ligand was then reacted with iron(III) chloride hydrate under reflux. No co-ligand was separately added to prepare complex **1**; however, an aqueous solution of sodium azide was used as a co-ligand for the preparation of complex **2**. Both complexes are stable at room temperature. The synthetic routes for both complexes are shown in Scheme 1.

### Description of the structures

**[FeL<sup>1</sup>Cl]·CH<sub>3</sub>CN (1).** Complex **1** crystallizes in the monoclinic space group  $P2_1/n$ . A perspective view of the complex with a selective atom-numbering scheme is shown in Fig. 1, and the ORTEP view is shown in Fig. S1 in the (ESI†). The asymmetric unit contains one discrete mononuclear iron(III) unit,  $[\text{FeL}^1\text{Cl}]$ , and one solvent acetonitrile molecule. The iron(III) center, Fe(1), has a six-coordinate pseudo-octahedral geometry. The deprotonated Schiff base ligand,  $(\text{L}^1)^{2-}$ , occupies five coordination sites by two imine nitrogen atoms, N(1) and N(3), one amine nitrogen atom, N(2), and two phenoxo oxygen atoms, O(1) and O(2). The remaining sixth coordination site is occupied by a chloride ion, Cl(3). Each of the two five-membered chelate rings {Fe(1)–N(1)–C(8)–C(9)–N(2)} and {Fe(1)–N(2)–C(10)–C(11)–N(3)} has a half-chair conformation with puckering parameters,<sup>19</sup>  $q = 0.471(2)$  Å,  $\varphi = 129.7(3)^\circ$  and  $q = 0.493(2)$  Å,  $\varphi = 309.0(3)^\circ$ , respectively. The deviations of the coordinating atoms, O(1), O(2), N(1) and N(2),



Scheme 1 Synthetic routes for complexes 1 and 2.

in the basal plane from the mean plane passing through them are  $-0.1825(17)$ ,  $0.1089(17)$ ,  $0.1555(18)$  and  $-0.158(218)$  Å, respectively, and the deviation of Fe(1) from the same plane is  $0.0757(3)$  Å.

**[FeL<sup>2</sup>(N<sub>3</sub>)] (2).** Complex 2 crystallizes in the monoclinic space group  $P2_1/n$ . The iron(III) center, Fe(1), has a six-coordinate pseudo-octahedral geometry. The deprotonated Schiff base ligand,  $(L^2)^{2-}$ , occupies five coordination sites by two imine nitrogen atoms, N(1) and N(3), one amine nitrogen atom, N(2), and two phenoxo oxygen atoms, O(1) and O(2), similar to that in complex 1. The remaining sixth coordination position is occupied by a nitrogen atom, N(4), of an azide. The perspective view of complex 2 is shown in Fig. 2 and the ORTEP view is shown in Fig. S2 (ESI<sup>†</sup>). Each of the two five-membered chelate rings {Fe(1)–N(1)–C(8)–C(9)–N(2)} and {Fe(1)–N(2)–C(10)–C(11)–N(3)} has a half-chair conformation with puckering parameters;<sup>19</sup>  $q = 0.457(4)$  Å,  $\varphi = 55.0(4)^\circ$  and  $q = 0.495(3)$  Å,  $\varphi = 227.5(4)^\circ$ , respectively. The deviations of the coordinating atoms, O(1), N(1), N(3) and N(4), in the basal plane from the mean plane passing through them are  $0.190(2)$ ,  $-0.221(3)$ ,  $0.156(3)$  and  $-0.224(4)$  Å, respectively, and the deviation of Fe(1) from the same plane is  $0.0984(5)$  Å.

### Supramolecular interactions

The solid state structures of both complexes 1 and 2 were stabilized through non-covalent hydrogen bonding interactions. In complex 1, one hydrogen atom, H(2A), attached to the amine nitrogen atom, N(2), formed an intermolecular hydrogen bonding interaction with the symmetry-related [ $a = 2 - x, 1 - y, 1 - z$ ] chloride, Cl(3)<sup>a</sup> (Fig. 3). On the other hand, one hydrogen atom, H(2A), attached to the amine nitrogen atom, N(2), in complex 2 formed a hydrogen bonding interaction with a symmetry-related ( $b = -x, 1 - y, 1 - z$ ) phenoxo oxygen atom, O(1)<sup>b</sup> (Fig. 4). Geometric features of the H-bonding interactions are given in Table 4.

The structure of complex 1 is additionally stabilized by significant  $\pi \cdots \pi$  stacking interactions. The phenyl rings, Cg(5) [C(1)–C(2)–C(3)–C(4)–C(5)–C(6)] and Cg(6) [C(13)–C(14)–C(15)–C(16)–C(17)–C(18)], undergo strong face-to-face  $\pi \cdots \pi$  stacking interactions with the neighboring phenyl rings Cg(6) [C(13)–C(14)–C(15)–C(16)–C(17)–C(18)], of symmetry  $(3/2 - x, 1/2 + y, 1/2 - z)$ , and Cg(5), [C(1)–C(2)–C(3)–C(4)–C(5)–C(6)], of symmetry  $(3/2 - x, -1/2 + y, 1/2 - z)$ , respectively. A one-dimensional array is formed *via* these  $\pi \cdots \pi$  stacking

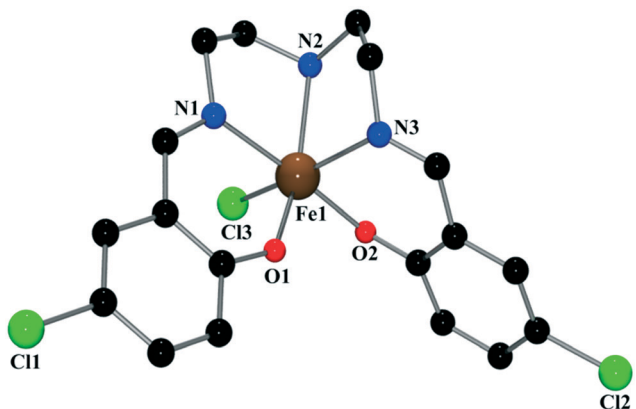


Fig. 1 Perspective view of complex 1 with selective atom numbering scheme. Hydrogen atoms and lattice acetonitrile molecule have been omitted for clarity.

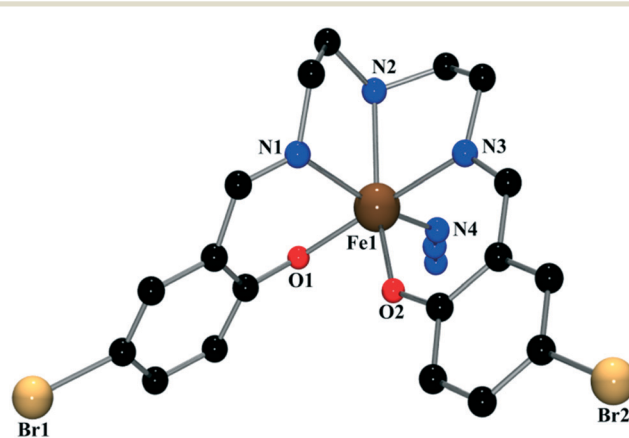


Fig. 2 Perspective view of complex 2 with selective atom numbering scheme. Hydrogen atoms have been omitted for clarity.

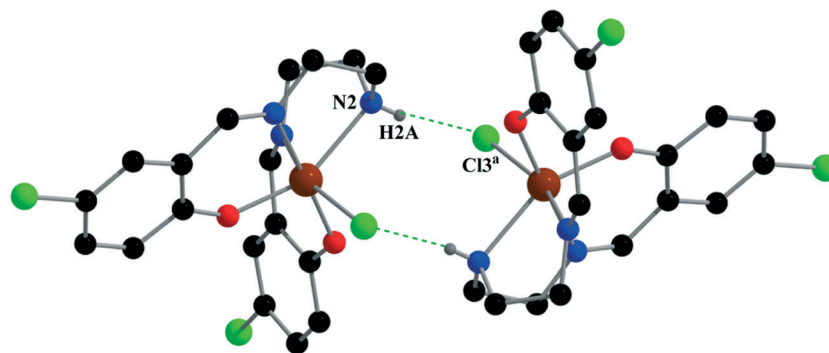


Fig. 3 A dimeric intermolecular hydrogen bonding interaction of complex 1. Only the relevant hydrogen atoms have been shown for clarity.  $a = 2 - x, 1 - y, 1 - z$ .

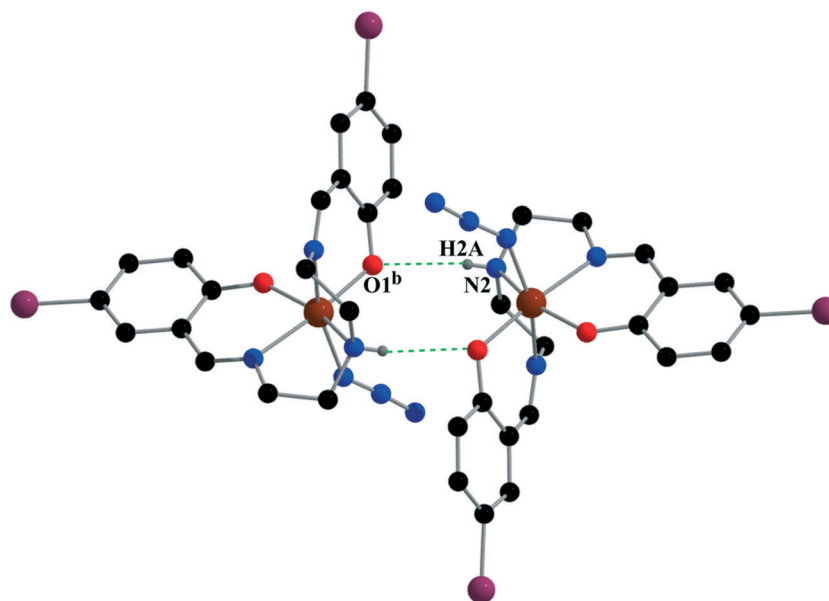


Fig. 4 A dimeric intermolecular hydrogen bonding interaction of complex 2. Only the relevant hydrogen atoms have been shown for clarity.  $b = -x, 1 - y, 1 - z$ .

Table 4 Hydrogen bond distances (Å) and angles ( $^{\circ}$ ) of complexes 1 and 2

Complex	D-H $\cdots$ A	D-H	H $\cdots$ A	D $\cdots$ A	$\angle$ D-H $\cdots$ A	Symmetry
1	N(2)-H(2A)-Cl(3)	0.72(3)	2.67(3)	3.329(2)	153(4)	$2 - x, 1 - y, 1 - z$
2	N(2)-H(2A)-O(1)	0.73(5)	2.37(5)	3.077(4)	162(5)	$-x, 1 - y, 1 - z$

Symmetry transformations:  $a = 2 - x, 1 - y, 1 - z$ ;  $b = -x, 1 - y, 1 - z$ .

interactions (Fig. 5). Geometric features of the  $\pi\cdots\pi$  stacking interactions are given in Table 5.

#### DFT study on supramolecular interactions

The theoretical study focused on analysis of the supramolecular dimers described above in Fig. 3 and 4, where N-H $\cdots$ Cl/N interactions are established. The energetic features of both dimers were compared. Moreover, in the case of complex 2, an interesting halogen bonding

interaction was studied, where the  $\sigma$ -hole at the Br atom interacts with the  $\pi$ -system of the organic Schiff-base ligand.

First of all, the molecular electrostatic potential (MEP) surfaces were computed for both complexes 1 and 2 to analyze their most electrophilic and nucleophilic parts. The MEP surfaces show that the maximum MEP values are located at the N-H groups of the Schiff-base ligands in both compounds (+44 kcal mol $^{-1}$ ). Moreover, the minimum MEP values are located at the anionic coligands (chlorido in 1 and azido in 2). The MEP values at the phenoxido O-atoms are

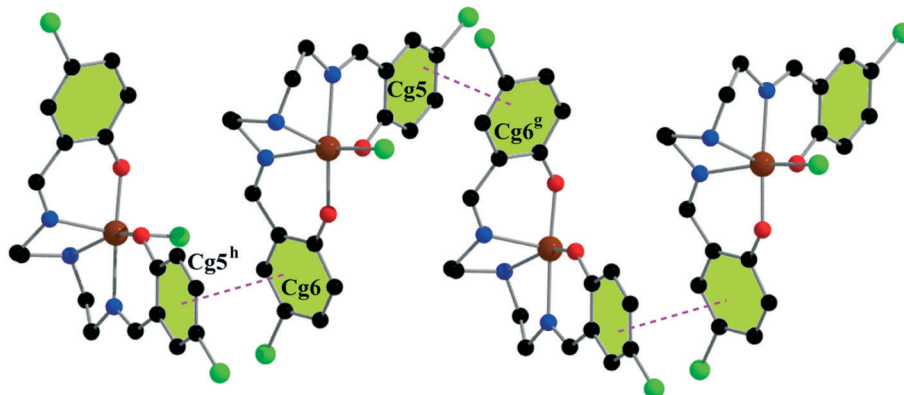


Fig. 5 One-dimensional array in complex **1**, generated through intermolecular  $\pi\cdots\pi$  stacking interactions. Only the relevant hydrogen atoms are shown for clarity.  $^g = 3/2 - x, 1/2 + y, 1/2 - z$ ;  $^h = 3/2 - x, -1/2 + y, 1/2 - z$ .

Table 5 Geometric features (distances in Å and angles in °) of the  $\pi\cdots\pi$  interactions obtained for complex **1**

Cg(I)⋯Cg(J)	Cg⋯Cg	$\alpha$	Cg(I)⋯Perp.	Cg(J)⋯Perp.
Cg(5)⋯Cg(6) <sup>g</sup>	3.9461(16)	21.18(12)	3.5825(10)	3.9234(11)
Cg(6)⋯Cg(5) <sup>h</sup>	3.9461(16)	21.18(12)	3.9234(11)	3.5825(10)

Symmetry transformation:  $^g = 3/2 - x, 1/2 + y, 1/2 - z$ ;  $^h = 3/2 - x, -1/2 + y, 1/2 - z$ .  $\alpha$ , dihedral angle between ring I and ring J; Cg(I)⋯Perp., perpendicular distance of Cg(I) on ring J; Cg(J)⋯Perp., perpendicular distance of Cg(J) on ring I; Cg(5) = C(1)–C(2)–C(3)–C(4)–C(5)–C(6); Cg(6) = C(13)–C(14)–C(15)–C(16)–C(17)–C(18).

–53 kcal mol<sup>–1</sup> in **1** and –41 kcal mol<sup>–1</sup> in **2**. This simple MEP analysis shows that the chlorido ligand is a better H-bond acceptor than the phenoxido O-atom, in agreement with the H-bonded dimer observed in the solid state of complex **1**. In the case of **2**, a similar agreement is not observed because the hydrogen bonds connect the N–H groups to the phenoxo oxygen atoms instead of the more negative azido ligands.

However, in this case, the MEP energy difference between the oxygen and nitrogen atoms is only 3 kcal mol<sup>–1</sup>, which can be easily compensated by other forces or crystal packing effects. The MEP surface of **1** also indicates that the aromatic chlorine presents a negligible  $\sigma$ -hole at the extension of the C–Cl bond (+0.95 kcal mol<sup>–1</sup>). In contrast, the  $\sigma$ -hole is more positive at the Br-atom in **2** (+7 kcal mol<sup>–1</sup>). The existence of

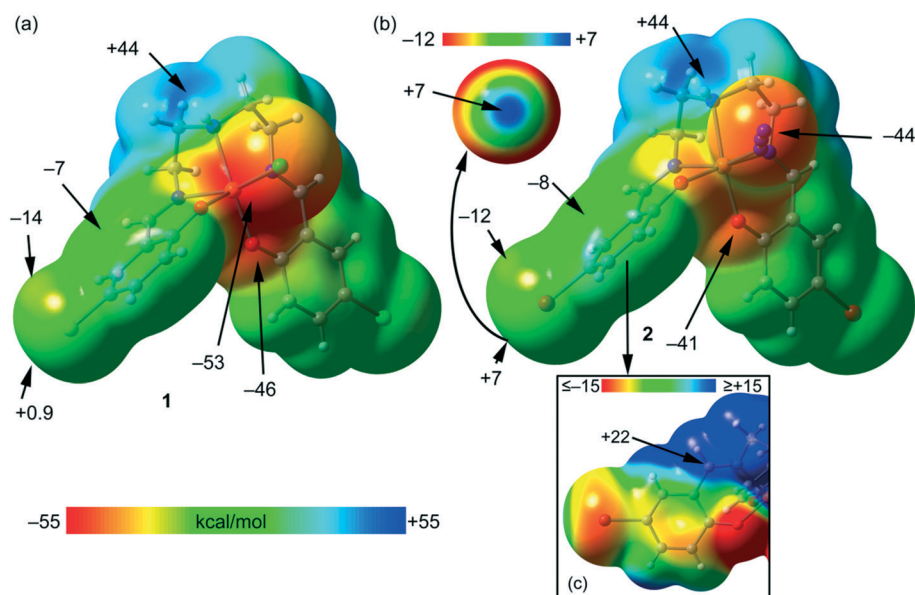


Fig. 6 MEP surfaces (isosurface 0.001 a.u.) of **1** (a) and **2** (b and c) at the PBE0-D3/def2-TZVP level of theory. The MEP values at selected points of the surface are indicated in kcal mol<sup>–1</sup>.

the  $\sigma$ -hole can be clearly observed if a reduced MEP scale is used (see Fig. 6b). The MEP surface also shows the typical negative belt around the bromine atom due to the presence of the three lone pairs. Finally, the MEP values over the center of the aromatic rings are negative in both compounds ( $-7$  kcal mol $^{-1}$  in **1** and  $-8.0$  kcal mol $^{-1}$  in **2**); thus, they are well suited for interacting with electron-poor regions such as H-atoms (C-H $\cdots\pi$  interactions) or the  $\sigma$ -hole of bromine ( $\sigma$ -hole $\cdots\pi$  or a halogen bond). Moreover, in Fig. 6c, an on-top representation of the aromatic ligand is given, also using a reduced scale ( $\pm 15$  kcal mol $^{-1}$ ). It can be appreciated that whilst the  $\pi$ -system of the aromatic ring presents a negative potential, the exocyclic imino group is positive; thus, it is well suited for interacting with negative regions.

Fig. 7 shows the energetic features of hydrogen-bonded dimers of **1** and **2** (see also Fig. 3 and 4 above). Moreover, the quantum theory of atoms in molecules (QTAIM) and non-covalent interaction plot (NCI plot) computational tools were used to describe and characterize the non-covalent bonds in both dimers, which are represented in Fig. 7. In the dimer of **1**, the distribution of critical points and bond paths reveals the presence of a network of hydrogen bonds (HBs) (C-H $\cdots$ O,Cl and N-H $\cdots$ O,Cl), each one characterized by the corresponding bond critical point (BCP) (red spheres labelled as **a-d** in Fig. 7a), bond path (dashed lines) and green isosurface (NCI plot) that interconnect each hydrogen atom to either Cl or O-atoms belonging to the chlorido or Schiff base ligand. This combination of interactions (eight HBs) justifies the large dimerization energy ( $\Delta E_1 = -29.0$  kcal mol $^{-1}$ ). In the dimer of **2**, the combined QTAIM/NCI plot analysis shows the formation of four hydrogen bonds (two C-H $\cdots$ N HBs and two N-H $\cdots$ O HBs, labelled as “e” and “f” in Fig. 7b, respectively), each one characterized by a BCP and bond path interconnecting the H atoms to the O/N-atoms. The QTAIM/NCI plot analysis also shows the existence of two symmetrically equivalent C-H $\cdots\pi$  (BCPs labelled as g) and lp $\cdots\pi$  interactions (labelled as h), characterized by the corresponding BCPs and green isosurfaces. That is, the lp $\cdots\pi$

interaction is characterized by a BCP and bond path interconnecting the nitrogen atom of the azido ligand to the carbon atom of the imino C=N bond of the Schiff base ligand. The formation of this interaction agrees well with the MEP surface shown in Fig. 6c, which shows a large and positive MEP value over the carbon atom of the imino group ( $+22$  kcal mol $^{-1}$ ); this is likely due to the coordination of the nitrogen atom to the metal center, which increases the electrophilicity of the carbon atom. The C-H $\cdots\pi$  interaction is characterized by a BCP and bond path interconnecting the hydrogen atom to one carbon atom of the aromatic ring of the Schiff base ligand. These additional interactions (C-H $\cdots\pi$  and lp $\cdots\pi$ ) justify the larger dimerization energy obtained for the dimer of **2** ( $\Delta E_2 = -32.8$  kcal mol $^{-1}$ ).

Finally, in complex **2**, the formation of a Br $\cdots\pi$  halogen bond observed in the solid state have also been analyzed. The combined QTAIM/NCI plot analysis of the dimer is shown in Fig. 8. The existence of the interaction is confirmed by both QTAIM and NCI plot computational tools. A BCP and bond path connects the bromine atom to one carbon atom of the aromatic ring. Moreover, the green isosurface located between the bromine atom and the carbon atom confirms the attractive nature of this interaction. This is in good agreement with the MEP surface of complex **2**, which shows the existence of a  $\sigma$ -hole at the Br-atom and a negative potential over the aromatic ring (see Fig. 6b). The dimerization energy of the dimer is modest ( $\Delta E_3 = -1.5$  kcal mol $^{-1}$ ), in line with the moderate positive MEP value at the  $\sigma$ -hole.

## IR and UV-vis spectra

The IR and electronic spectra of both complexes are in good agreement with their corresponding crystal structures. A strong band at  $\sim 1618$  cm $^{-1}$  is observed in the IR spectrum of each complex. This band indicates the presence of the azomethine (C=N) functionality, as expected to be present in Schiff base complexes.<sup>20</sup> In the case of complex **1**, there is a small sharp peak at 2066 cm $^{-1}$ , which corresponds to

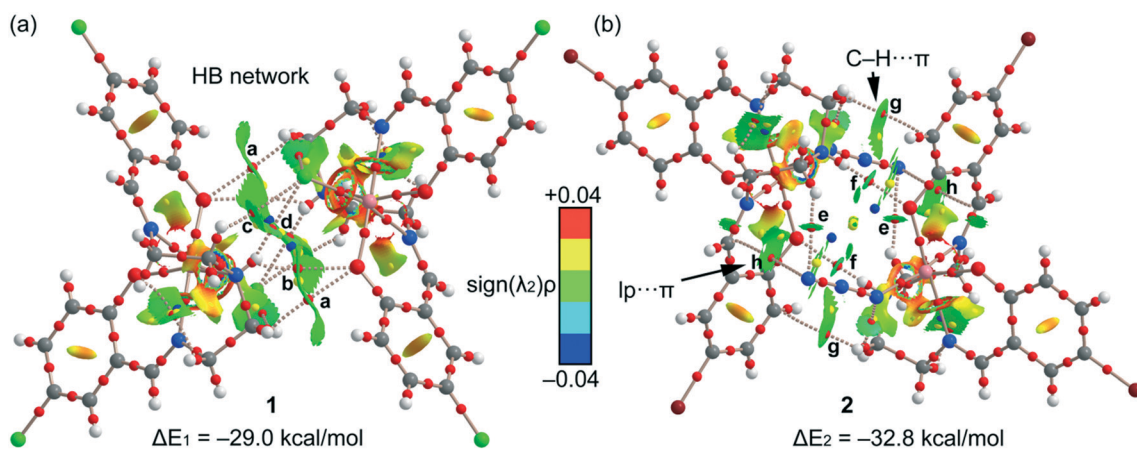


Fig. 7 Combined QTAIM (bond, ring and cage critical points are represented as red, yellow and blue spheres, respectively) and NCI plot analyses of the dimers of **1** (a) and **2** (b). The BSSE-corrected dimerization energies are also indicated.

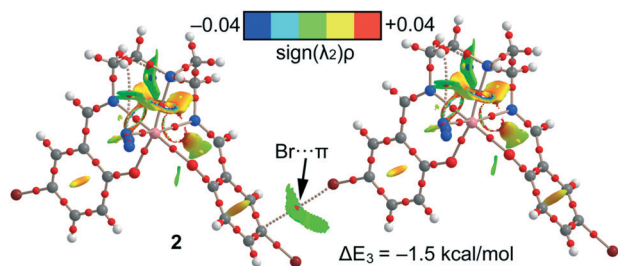


Fig. 8 Combined QTAIM (bond and ring critical points are in red and yellow, respectively) and NCI plot analyses of the Br $\cdots$  $\pi$  dimer of **2**.

the presence of the nitrile group (C $\equiv$ N) of the solvent acetonitrile molecule. A sharp band at around 2050 cm $^{-1}$  in the IR spectrum of complex **2** corresponds to the terminal azide.<sup>21</sup> For both complexes, characteristic small bands of the N–H stretching vibrations are located in the interval of 3230–3220 cm $^{-1}$ . The band is broader in complex **2**, as the N–H bond is involved in H-bonding interactions with the phenoxy oxygen atom of a symmetry-related neighbouring molecule. On the other hand, bending N–H vibrations are located in the region of 1530–1520 cm $^{-1}$ .<sup>22</sup> The bands in the ranges of 2942–2968 cm $^{-1}$  and 1450–1460 cm $^{-1}$  are due to the stretching and bending vibrations of C–H bonds.<sup>23</sup> Both C–Cl ( $\sim$ 850 cm $^{-1}$ ) and C–Br ( $\sim$ 679 cm $^{-1}$ ) stretching frequencies are observed in the lower wave number region. Characteristic bands of the C–H $\cdots$ halogen hydrogen bond are observed in the range of 1330–1280 cm $^{-1}$ .<sup>23b</sup> The IR spectra of both complexes **1** and **2** are shown in Fig. S3 and S4 (ESI $^\dagger$ ).

The electronic spectra of the two complexes are similar in nature. The spectrum for each complex consists of three distinct bands at  $\sim$ 500 nm,  $\sim$ 300 nm and  $\sim$ 225 nm. The d–d transitions in high-spin iron(III) in an octahedral field (with  $^6A_{1g}$  ground state) should be very weak, as they are strictly spin forbidden (and obviously Laporte forbidden as well); therefore, they are not observed. The observed peaks in the electronic spectra may therefore be considered to originate from charge transfer transitions. The bands (of very low intensity) corresponding to the d  $\rightarrow$  d transitions are actually obscured by these high intensity charge transfer bands. In the case of complex **1**, the band at 501 nm can be assigned to the azide-to-iron(III) charge transfer (CT) transition,<sup>24</sup> and in complex **2**, a similar band is observed at 490 nm due to the chlorine-to-iron(III) charge transfer (CT) transition.<sup>24</sup> A moderately stronger band is observed around 319 nm with a shoulder at 368 nm; these can tentatively be assigned to superpositions of the amine-to-iron(III) and phenoxy-to-iron(III) CT, respectively.<sup>25</sup> Similarly, complex **2** shows this type of band around 309 nm with a shoulder at 361 nm due to the same reason mentioned above. For both complexes, the bands around 225 nm can be assigned to intra-ligand  $\pi \rightarrow \pi^*$  transitions.<sup>26</sup> The band positions and intensities are comparable with those found in similar complexes.<sup>24–26</sup> UV-vis spectra of both complexes **1** and **2** are shown in Fig. S5 (ESI $^\dagger$ ).

## Conclusions

Two triamine-based Schiff base complexes have been synthesised and characterised. In the solid state, both complexes form self-assembled H-bonded dimers, which have been studied by means of DFT calculations. The non-covalent contacts have also been characterized by a combination of QTAIM and NCI plot computational tools. The formation of the dimer is more favorable in complex **2** due to the formation of ancillary C–H $\cdots$  $\pi$  and lp $\cdots$  $\pi$  interactions. Finally, the formation of a weak Br $\cdots$  $\pi$  halogen bond in complex **2** has been studied. The existence of a  $\sigma$ -hole at the bromine atom and the attractive nature of this contact has been evidenced by both DFT energetic calculations and NCI plot analysis.

## Conflicts of interest

No conflicts of interest to declare.

## Acknowledgements

T. B. thanks the CSIR, India, for awarding a Senior Research Fellowship [Sanction No. 09/096(0861)/2016-EMR-I]. S. C. gratefully acknowledges UGC-CAS II program, Department of Chemistry, Jadavpur University, for financial support under the head [Chemicals/Consumables/Glassware]. A. F. thanks the MICIU/AEI from Spain for financial support (Project CTQ2017-85821-R, Feder funds) and the CTI (UIB) for computational facilities.

## References

- (a) C. O. Rodriguez de Barbarin, N. A. Bailey, D. E. Fenton and Q.-Y. He, *J. Chem. Soc., Dalton Trans.*, 1997, 161; (b) E. J. Larson and V. L. Pecoraro, *J. Am. Chem. Soc.*, 1991, **113**, 3810; (c) M. M. Taqui Khan, D. Srinivas, R. I. Kureshi and N. H. Khan, *Inorg. Chem.*, 1990, **29**, 2320; (d) H. Miyasaka, H. Ieda, N. Mastumoto, R. Crescenzi and C. Floriani, *Inorg. Chem.*, 1998, **37**, 255; (e) I. Ramade, O. Khan, Y. Jennin and F. Robert, *Inorg. Chem.*, 1997, **36**, 930; (f) D. Wohrle, *Adv. Polym. Sci.*, 1983, **50**, 45; (g) N. Hoshino, *Coord. Chem. Rev.*, 1998, **174**, 77.
- (a) M. J. Prushan, D. M. Tomezsko, S. Lofland, M. Zeller and A. D. Hunter, *Inorg. Chim. Acta*, 2007, **360**, 2245; (b) S. Chattopadhyay, M. G. B. Drew and A. Ghosh, *Eur. J. Inorg. Chem.*, 2008, 1693; (c) M. Ghiladi, J. T. Gomez, A. Hazell, P. Kofod, J. Lumtscher and C. J. McKenzie, *Dalton Trans.*, 2003, 1320.
- (a) J. C. Fanning, J. L. Resce, G. C. Lickfield and M. E. Kotun, *Inorg. Chem.*, 1985, **24**, 2884; (b) K. C. Gupta and A. K. Sutar, *Coord. Chem. Rev.*, 2008, **252**, 1420–1450; (c) V. Mirkhani, M. Moghadam, S. Tangestaninejad, I. M. Baltork and N. Rasouli, *Inorg. Chem. Commun.*, 2007, **10**, 1537–1540; (d) J. Li, J. Yang, Y.-Y. Liu and J.-F. Ma, *Chem. – Eur. J.*, 2015, **21**, 4413–4421.
- (a) D. M. Kurtz, *Chem. Rev.*, 1990, **90**, 585; (b) B. J. Wallar and J. D. Lipscomb, *Chem. Rev.*, 1996, **96**, 2625; (c) E. I.

- Solomon, T. C. Brunold, M. I. Davis, J. N. Kemsley, S.-K. Lee, N. Lehnert, F. Neese, A. J. Skulan, Y.-S. Yang and J. Zhou, *Chem. Rev.*, 2000, **100**, 235.
- 5 (a) S. Jana, S. Chatterjee and S. Chattopadhyay, *Polyhedron*, 2012, **48**, 189–198; (b) T. Basak, K. Ghosh and S. Chattopadhyay, *Polyhedron*, 2018, **146**, 81–92; (c) T. Basak, K. Ghosh, C. J. Gómez-García and S. Chattopadhyay, *Polyhedron*, 2018, **146**, 42–54.
- 6 (a) T. Basak, D. Das, P. P. Ray, S. Banerjee and S. Chattopadhyay, *CrystEngComm*, 2020, **22**, 5170–5181; (b) T. Basak, A. Frontera and S. Chattopadhyay, *CrystEngComm*, 2020, **22**, 5731–5742.
- 7 (a) A. Majumder, G. Pilet, M. T. G. Rodriguez and S. Mitra, *Polyhedron*, 2006, **25**, 2550–2558; (b) A. Lavalette, F. Tuna, G. Clarkson, N. W. Alcock and M. J. Hannon, *Chem. Commun.*, 2003, 2666–2667; (c) F. Grimm, N. Ulm, F. Grçhn, J. Dring and A. Hirsch, *Chem. – Eur. J.*, 2011, **17**, 9478–9488; (d) H. T. Chifotides and K. R. Dunbar, *Acc. Chem. Res.*, 2013, **46**, 894–906; (e) X. Zhao, H. He, F. Dai, D. Sun and Y. Ke, *Inorg. Chem.*, 2010, **49**, 8650–8652; (f) N. Yoshida, N. Yoshida, H. Oshio and T. Ito, *Chem. Commun.*, 1998, 63–64; (g) T. Clark, M. Hennemann, J. S. Murray and P. Politzer, *J. Mol. Model.*, 2007, **13**, 291; (h) P. Politzer, J. S. Murray and T. Clark, *Phys. Chem. Chem. Phys.*, 2013, **15**, 11178; (i) J. S. Murray, P. Lane, T. Clark, K. E. Riley and P. Politzer, *J. Mol. Model.*, 2012, **18**, 541; (j) T. J. Mooibroek, P. Gamez and J. Reedijk, *CrystEngComm*, 2008, **10**, 1501; (k) I. Alkorta, J. Elguero and A. Frontera, *Crystals*, 2020, **10**, 180; (l) A. Bauzá, I. Alkorta, J. Elguero, T. J. Mooibroek and A. Frontera, *Angew. Chem., Int. Ed.*, 2020, **59**, 17482–17487.
- 8 (a) P. Politzer, J. S. Murray and T. Clark, *Phys. Chem. Chem. Phys.*, 2013, **15**, 11178–11189; (b) A. Bauza, T. J. Mooibroek and A. Frontera, *ChemPhysChem*, 2015, **16**, 2496–2517; (c) A. Bauza and A. Frontera, *Angew. Chem., Int. Ed.*, 2015, **54**, 7340–7343.
- 9 G. M. Sheldrick, *Acta Crystallogr., Sect. C: Struct. Chem.*, 2015, **71**, 3–8.
- 10 G. M. Sheldrick, *SADABS, V2014/5, Software for Empirical Absorption Correction*, University of Göttingen, Institute für Anorganische Chemieder Universität, Göttingen, Germany, 1999–2003.
- 11 M. J. Frisch, G. W. Trucks, H. B. Schlegel, G. E. Scuseria, M. A. Robb, J. R. Cheeseman, G. Scalmani, V. Barone, G. A. Petersson, H. Nakatsuji, X. Li, M. Caricato, A. Marenich, J. Bloino, B. G. Janesko, R. Gomperts, B. Mennucci, H. P. Hratchian, J. V. Ortiz, A. F. Izmaylov, J. L. Sonnenberg, D. Williams-Young, F. Ding, F. Lipparini, F. Egidi, J. Goings, B. Peng, A. Petrone, T. Henderson, D. Ranasinghe, V. G. Zakrzewski, J. Gao, N. Rega, G. Zheng, W. Liang, M. Hada, M. Ehara, K. Toyota, R. Fukuda, J. Hasegawa, M. Ishida, T. Nakajima, Y. Honda, O. Kitao, H. Nakai, T. Vreven, K. Throssell, J. A. Montgomery Jr., J. E. Peralta, F. Ogliaro, M. Bearpark, J. J. Heyd, E. Brothers, K. N. Kudin, V. N. Staroverov, T. Keith, R. Kobayashi, J. Normand, K. Raghavachari, A. Rendell, J. C. Burant, S. S. Iyengar, J. Tomasi, M. Cossi, J. M. Millam, M. Klene, C. Adamo, R. Cammi, J. W. Ochterski, R. L. Martin, K. Morokuma, O. Farkas, J. B. Foresman and D. J. Fox, *Gaussian 16 (Revision A.03)*, Gaussian Inc., Wallingford CT, 2016.
- 12 S. B. Boys and F. Bernardi, *Mol. Phys.*, 1970, **19**, 553–566.
- 13 S. Grimme, J. Antony, S. Ehrlich and H. Krieg, *J. Chem. Phys.*, 2010, **132**, 154104.
- 14 (a) P. Manna, S. K. Seth, M. Mitra, S. Ray Choudhury, A. Bauzá, A. Frontera and S. Mukhopadhyay, *Cryst. Growth Des.*, 2014, **14**, 5812–5821; (b) M. Mirzaei, H. Eshtiagh-Hosseini, Z. Bolouri, Z. Rahmati, A. Esmaeilzadeh, A. Bauza, P. Ballester, M. Barceló-Oliver, J. T. Mague, B. Notash and A. Frontera, *Cryst. Growth Des.*, 2015, **15**, 1351–1361; (c) S. Mirdaya, M. G. B. Drew, A. K. Chandra, A. Banerjee, A. Frontera and S. Chattopadhyay, *Polyhedron*, 2020, **179**, 114374; (d) P. Sharma, A. Gogoi, A. K. Verma, A. Frontera and M. K. Bhattacharyya, *New J. Chem.*, 2020, **44**, 5473–5488; (e) B. Chowhan, M. Gupta, N. Sharma and A. Frontera, *J. Mol. Struct.*, 2020, **1207**, 127785; (f) P. Kar, A. Franconetti, A. Frontera and A. Ghosh, *CrystEngComm*, 2019, **21**, 6886–6893; (g) A. Gogoi, D. Dutta, A. K. Verma, H. Nath, A. Frontera, A. K. Guha and M. K. Bhattacharyya, *Polyhedron*, 2019, **168**, 113–126; (h) A. Banerjee, A. Frontera and S. Chattopadhyay, *Dalton Trans.*, 2019, **48**, 11433–11447; (i) T. Hajiashrafi, S. Salehi, M. Kubicki, A. Bauzá, A. Frontera, K. J. Flanagan and M. O. Senge, *CrystEngComm*, 2019, **21**, 6301–6312; (j) M. K. Bhattacharyya, A. Gogoi, S. Chetry, D. Dutta, A. K. Verma, B. Sarma, A. Franconetti and A. Frontera, *J. Inorg. Biochem.*, 2019, **200**, 110803; (k) S. Mirdaya, S. Roy, S. Chatterjee, A. Bauzá, A. Frontera and S. Chattopadhyay, *Cryst. Growth Des.*, 2019, **19**, 5869–5881; (l) S. Dutta, S. Chakraborty, M. G. B. Drew, A. Frontera and A. Ghosh, *Cryst. Growth Des.*, 2019, **19**, 5819–5828; (m) K. Das, S. Goswami, B. B. Beyene, A. W. Yibeltal, C. Massera, E. Garribba, A. Frontera, Z. Cantürk, T. Askun and A. Datta, *Inorg. Chim. Acta*, 2019, **490**, 155–162; (n) I. Mondal, K. Ghosh, A. Franconetti, A. Frontera, S. Chatterjee and S. Chattopadhyay, *J. Coord. Chem.*, 2019, **72**, 3237–3247; (o) A. Radha, S. Kumar, D. Sharma, A. K. Jassal, J. K. Zaręba, A. Franconetti, A. Frontera, P. Sood and S. K. Pandey, *Polyhedron*, 2019, **173**, 114126; (p) S. Mirdaya, A. Frontera and S. Chattopadhyay, *CrystEngComm*, 2019, **21**, 6859–6868; (q) D. Dutta, S. M. Nashre-ul-Islam, U. Saha, A. Frontera and M. K. Bhattacharyya, *J. Mol. Struct.*, 2019, **1195**, 733–743; (r) M. Kazmi, A. Ibrar, H. S. Ali, M. Ghufuran, A. Wadood, U. Flörke, J. Simpson, A. Saeed, A. Frontera and I. Khan, *J. Mol. Struct.*, 2019, **1197**, 458–470.
- 15 R. F. W. Bader, *J. Phys. Chem.*, 1998, **102**, 7314–7323.
- 16 J. Contreras-Garcia, E. Johnson, S. Keinan, R. Chaudret, J.-P. Piquemal, D. Beratan and W. Yang, *J. Chem. Theory Comput.*, 2011, **7**, 625–632.
- 17 T. A. Keith, *AIMAll (Version 19.02.13)*, TK Gristmill Software, Overland Park KS, USA, 2019, (aim.tkgristmill.com).
- 18 I. Nemeč, R. Herchel, R. Boca, Z. Travnicek, I. Svoboda, H. Fuessd and W. Linert, *Dalton Trans.*, 2011, **40**, 10090–10099.
- 19 (a) D. Cremer and J. A. Pople, *J. Am. Chem. Soc.*, 1975, **97**, 1354–1358; (b) D. Cremer, *Acta Crystallogr., Sect. B: Struct. Sci.*, 1984, **40**, 498–500.

- 20 L. Pogany, J. Moncol, J. Pavlik and I. Salitros, *New J. Chem.*, 2017, **41**, 5904–5915.
- 21 (a) S. Mirdya, T. Basak and S. Chattopadhyay, *Polyhedron*, 2019, **170**, 253–263; (b) S. Roy, S. Halder, A. Dey, K. Harms, P. P. Ray and S. Chattopadhyay, *New J. Chem.*, 2020, **44**, 1285–1293.
- 22 M. Karmakar, T. Basak and S. Chattopadhyay, *New J. Chem.*, 2019, **43**, 4432–4443.
- 23 (a) T. Basak, A. Bhattacharyya, M. Das, K. Harms, A. Bauza, A. Frontera and S. Chattopadhyay, *ChemistrySelect*, 2017, **2**, 6286–6295; (b) S. Saha, L. Rajput, S. Joseph, M. K. Mishra, S. Ganguly and G. R. Desiraju, *CrystEngComm*, 2015, **17**, 1273–1290.
- 24 (a) S. Naiya, M. G. B. Drew, C. Diaz, J. Ribas and A. Ghosh, *Eur. J. Inorg. Chem.*, 2011, 4993–4999; (b) S. Naiya, S. Giri, S. Biswas, M. G. B. Drew and A. Ghosh, *Polyhedron*, 2014, **73**, 139–145.
- 25 (a) R. Biswas, C. Diaz, A. Bauzá, A. Frontera and A. Ghosh, *Dalton Trans.*, 2013, **42**, 12274–12283; (b) S. Jana, A. Bhattacharyya, B. N. Ghosh, K. Rissanen, S. Herrero, R. J. Aparicio and S. Chattopadhyay, *Inorg. Chim. Acta*, 2016, **453**, 715–723; (c) F. Banse, V. Balland, C. Philouze, E. Riviere, L. Tchertanova and J.-J. Girerd, *Inorg. Chim. Acta*, 2003, **353**, 223–230.
- 26 R. Biswas, M. G. B. Drew, C. Estarellas, A. Frontera and A. Ghosh, *Eur. J. Inorg. Chem.*, 2011, 2558–2566.